38th ERF, September 4–7, 2012, Amsterdam, The Netherlands

040
Experimental Method for Drag Measurement of an Oscillating Airfoil in Dynamic Stall Condition

G. Gibertini*, F. Auteri, D. Grassi, D. Spreafico and A. Zanotti

Dipartimento di Ingegneria Aerospaziale – Politecnico di Milano
Via La Masa 34, 20156 Milano – Italy
e–mail: *giuseppe.gibertini@polimi.it

Keywords: Aerodynamics, Oscillating airfoil, Phase Average, Hot-wire anemometry.

Abstract

The paper describes an experimental activity carried out on an oscillating airfoil in dynamic stall condition. In particular, the wake of the pitching model was measured by means of a triple hot-wire probe sweeping the test section height. The extensive test campaign investigates the wake of an oscillating airfoil in the different regimes of dynamic stall (Light and Deep dynamic stall) producing a comprehensive experimental data base that could be considered a reference for the validation of CFD tools. Moreover, a preliminar study to determine the periodic drag acting on the oscillating airfoil is presented. The drag is obtained by integration of flow field measurements: the method relies upon the application of the control volume approach in combination with the phase averaging of the quantities involved.

Nomenclature

α	angle of attack [deg]
α_m	mean angle of attack [deg]
α_a	pitching oscillation amplitude [deg]
ω	circular frequency [rad/s]
b	blade section model span [m]
c	blade section model chord [m]
C_D	drag coefficient
f	oscillation frequency [Hz]
h	test section height [m]
HW	Hot-Wire
k	reduced frequency $= \pi fc/U_\infty$
Ma	Mach number
PIV	Particle Image Velocimetry
q_∞	free-stream dynamic pressure [Pa]
Re	Reynolds number
U	velocity component in free-stream direction [m/s]
U_∞	free-stream velocity [m/s]

1 Introduction

The dynamic stall phenomenon has become in the recent years one of the more investigated topics in rotorcraft aerodynamics and aeroelasticity fields due to the strong demand for faster helicopters. In particular, the main goal of the research activities is to overcome the dynamic stall on the retreating blade that limits the high speed performance of classical helicopter rotor configurations [1, 2]. Consequently, the investigation of the fine details involved in this phenomenon has become the object of several experimental and numerical activities [3, 4].

In particular, the object of the experimental activity carried out at Politecnico di Milano was the characterisation of the wake of an oscillating airfoil in dynamic stall conditions [5, 6]. The activity presented in this paper was conducted in the frame of research about the dynamic stall on the retreating helicopter blade, currently involving both experimental and numerical specialists in our department. In particular, the wake of the pitching blade section model was measured by means of a triple hot-wire probe. The test campaign investigates the different regimes of dynamic stall occurring on the rotor retreating blade in forward flight (Light Dynamic Stall and Deep Dynamic Stall). The comprehensive data base produced by the experimental activity could be considered an interesting reference to validate CFD tools for these peculiar unsteady flow conditions.

The wind tunnel tests have been carried out at the Aerodynamics Laboratory of Politecnico di Milano, using an experimental rig designed for testing full scale helicopter blade sections oscillating in pitch. The experimental set up is also suitable for unsteady pressure measurements on the blade midspan airfoil contour, in order to evaluate the airloads acting on the blade during the pitching cycle. The test campaign included pressure measurements on the ceiling and on the floor of the wind tunnel. Pressure and velocity measurements were used in a preliminary study for the evaluation of the total drag component acting on the oscillating airfoil. In fact, pressure and velocity surveys can be used, as an alternative to the use of wind tunnel balance, to measure the aerodynamic forces and moment acting on a wing section. In fact, model wall pressure integration can be used to determine lift and pitching moment while the integration of the wake momentum defect can be used to obtaine the drag value. Methods proposed in the past by Betz [7] and Jones [8] for steady flow conditions are widely used and the recent paper by van Dam [9] presented an exhaustive review.

The evaluation of the total drag for a pitching airfoil in dynamic stall conditions can be considered a very challenging goal, in fact, the experimental works in literature present only the measurement of the pressure drag component obtained by the integration of pressure on the airfoil contour [11]. The present work illustrates preliminary results about total drag component evaluation obtained by the integration of flow field measurements and the use of the phase averaging of the quantities involved.

2 Experimental set up

The experimental activity was conducted at Politecnico di Milano in the low-speed closed-return wind tunnel of the Aerodynamics Laboratory of the Aerospace Department. The wind tunnel has a rectangular test section with 1.5 m height and 1 m width. The maximum wind velocity is 55 m/s and the freestream turbulence level is less than 0.1%.

For this activity a NACA 23012 aluminium machined model, with chord $c = 0.3$ m and span $b = 0.93$ m was used. The model has an interchangeable midspan section for the different measurements techniques employed. One of the available central sections is equipped with pressure taps positioned along the midspan chord line and instrumented with 21 Kulite fast-response pressure transducers. The time history of the pressure drag component during a pitching cycle was evaluated by integration of the phase averaged pressures collected over 30 complete pitching cycles.

The model is pivoted around the axis at 25% of the airfoil chord by a brushless servomotor with a 12:1 gear drive. A more detailed description of the pitching airfoil experimental rig and of the measurement techniques set up can be found in Zanotti et al. [10].

Figure 1 illustrates the blade section model

Figure 1: NACA 23012 blade section model inside the wind tunnel test section.

inside the wind tunnel; behind the model the supporting strut for the triple hot wire probe can be observed.

2.1 Hot wire measurement set up

The velocity surveys in the wake of the oscillating airfoil were carried out by means of a Constant Temperature Anemometry (CTA) system Streamline 90N10 by Dantec Dynamics. The system was composed by one frame with three CTA modules. Every basic anemometer module contains three CTA bridges, a servo-loop with programmable gain, filters and cable compensation and a programmable signal conditioner. The programmable servo-loop allows to optimize the dynamic response and the bandwidth of the system, while the signal conditioner provides amplification of the CTA signal before digitizing.

A tri-axial fiber-film probe Dantec 55R91 was used for the velocity surveys. The tri-axial sensor probe has three mutually perpendicular sensors, consisting of fiber films. The sensors form an orthogonal system with an acceptance cone of 70.4°. Figure 2 shows a particular of the triple HW probe inside the test section.

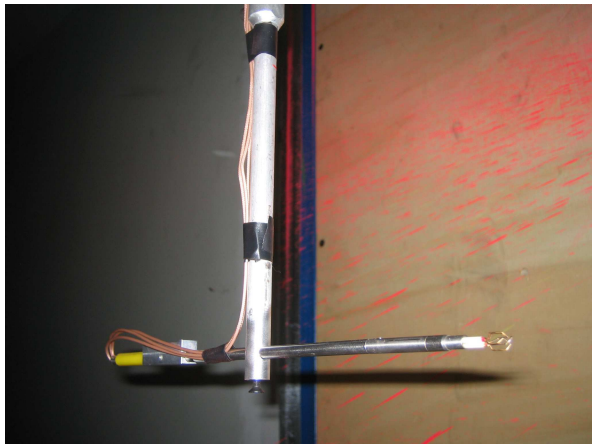

Figure 2: Tri-axial HW probe inside the wind tunnel tests section in PIV mode.

The probe is moved in the model midspan plane along the test section height direction by means of a single axis traversing system. The velocity profile was measured 2 chords past the airfoil trailing edge. The velocity time history was acquired for a time corresponding to 150 complete pitching cycles with a sampling frequency of 20 kHz.

2.2 Pressure measurement set up

Pressure on the test section ceiling and floor was measured by means of a pressure rod (see Fig. 3(a)) instrumented with two Kulite fast response transducers (2 PSI F.S.) and successively mounted on the ceiling and on the floor. Pressure ports are located on the longitudinal midspan plane of the rod, while the transducers are installed in a threaded housing on the lateral side of the rod (see the particular of the layout in Fig. 3(b).

Pressure was measured in correspondence of two pressure ports located 2 chords downstream the airfoil trailing edge (longitudinal position of the HW velocity surveys) and 3 chords upstream the airfoil leading edge.

3 Phase Averaging Method

The phase averaging is the most widely used method to point out a time-varying signal measured in case of periodic unsteady flows. The

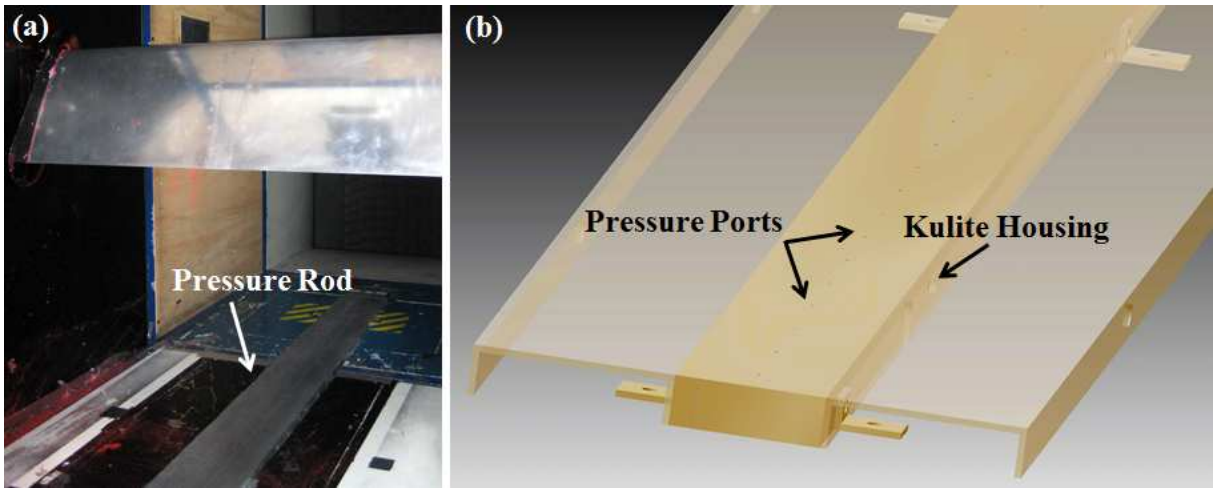

Figure 3: (a) Aluminium rod for pressure measurements installed in the test section; (b) Particular of the pressure rod layout.

measured time-varying signal $s(t)$ can be decomposed as follows

$$s(t) = \langle s(t) \rangle + s'(t) \tag{1}$$

into a phase average term $\langle s(t) \rangle$ and a fluctuating term $s'(t)$. The phase averaging operator is defined as follows:

$$\langle s(t) \rangle = \lim_{N \to \infty} \frac{1}{N} \sum_{i=1}^{N} s(t + (i-1)T), \tag{2}$$

where T is the period of the cyclic flow and N the number of cycles, while the fluctuations term is defined as

$$s'(t) = s(t) - \langle s(t) \rangle. \tag{3}$$

In practice, the phase average term depends also on the number of cycles N as the phase averaging method is carried out over a finite number of cycles. Then the definition of the phase average term in Eq.(2) becomes

$$\langle s(t, N) \rangle = \frac{1}{N} \sum_{i=1}^{N} s(t + (i-1)T). \tag{4}$$

The larger is the number of cycles N, the more converging is the $\langle s(t, N) \rangle$ value towards the theoretical phase average term $\langle s(t) \rangle$. The criterion to determine the number of cycles to be used in the phase averaging method has been discussed by Wernert and Favier [13] for different measurement techniques.

4 Wake velocity surveys results

The two conditions considered for wake velocity surveys are sinusoidal pitching cycles with reduced frequency $k = 0.1$, oscillation amplitude $\alpha_a = 10°$ and a mean angle of attack $\alpha_m = 5°$ (light dynamic stall) and $\alpha_m = 10°$ (deep dynamic stall). The tests were carried out at $U_\infty = 30$ m/s, corresponding to a Reynolds number of Re $= 6 \times 10^5$ and a Mach number of Ma $= 0.09$.

Figures 4 and 5 present the phase averaged free-stream velocity component profiles measured in the wake of the oscillating airfoil for some interesting angles of attack in the two tested conditions.

For the light dynamic stall condition, the measured velocity profiles show a small defect of the freestream velocity component extended over a small spatial amplitude along the test section height, both in upstroke and in downstroke (see Fig. 4). These considerations support the fact that in this dynamic stall regime the flow on the upper surface of the airfoil is attached for almost all the pitching cycle.

In the upstroke phase the two tested conditions present similar characteristics of the velocity profiles. In fact, for the test case with $\alpha_m = 10°$ the stall is delayed at an angle of attack higher than the static stall angle corresponding to ($\alpha \approx 15°$) by the effect of the

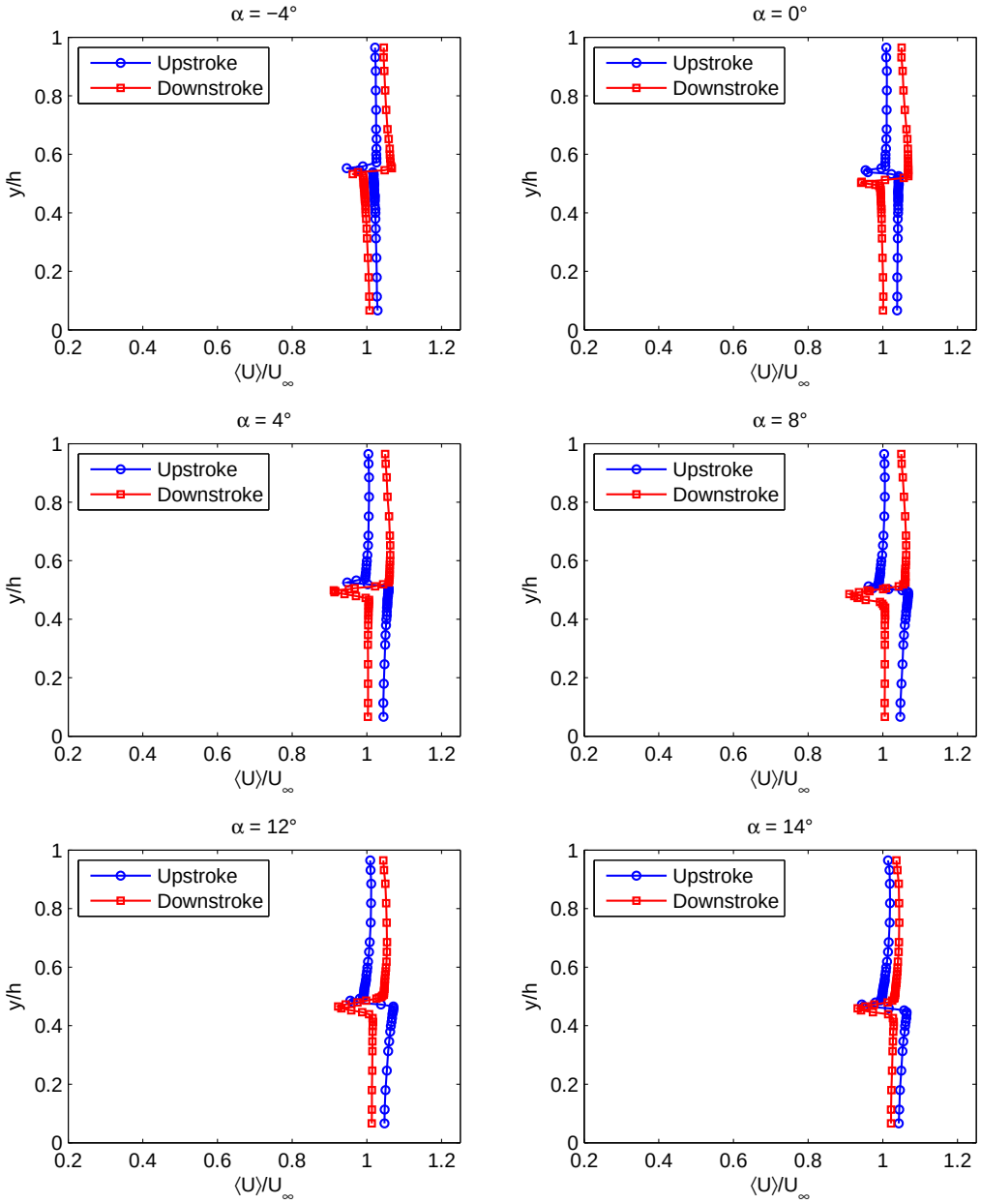

Figure 4: Streamwise velocity profiles for $\alpha = 5° + 10° \sin(\omega t)$, $k = 0.1$ (Re $= 6 \times 10^5$ and Ma $= 0.09$)

rapid positive pitching rate and consequently the flow separation starts only at the end of the upstroke motion ($\alpha \approx 19°$) as illustrated by PIV measurements described in Zanotti et al. [12].

During the downstroke motion, the flow field presents a massive separation on the airfoil upper surface and is characterised by the formation and migration of strong vortices. In fact, the measured velocity profiles show a higher velocity defect that is extended for about half of the test section height for $\alpha = 15°$ (see Fig. 5). The huge velocity defect measured for this angle of attack is due to the passage of a strong

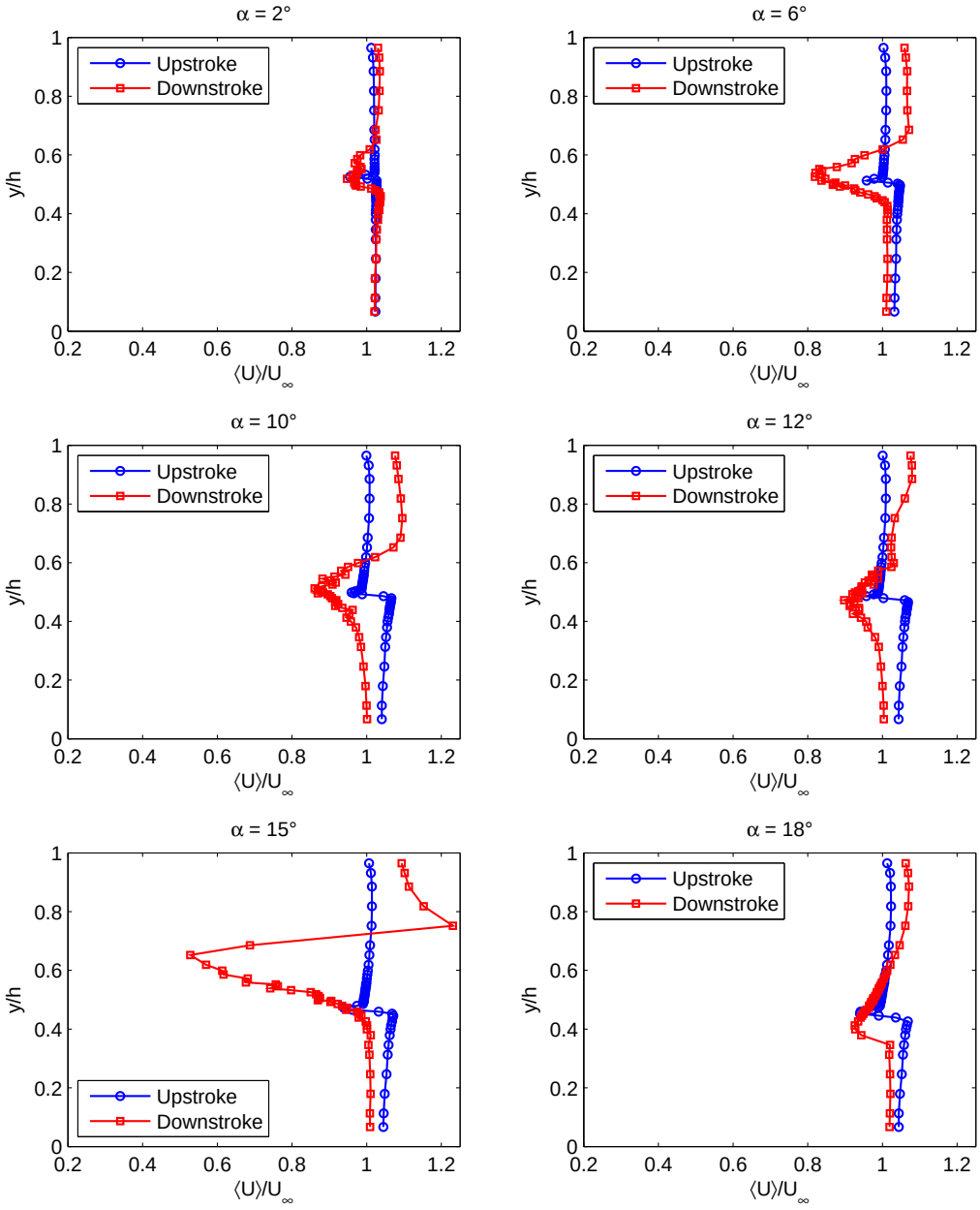

Figure 5: Streamwise velocity profiles for $\alpha = 10^\circ + 10^\circ \sin(\omega t)$, $k = 0.1$ (Re $= 6 \times 10^5$ and Ma $= 0.09$)

vortical structure that starts on the airfoil upper surface at the beginning of the downstroke (see PIV measurements described in Zanotti et al. [12]). The large height of the velocity defect region measured 2 chords past the airfoil trailing edge is measured with a delay in angle of attack with respect to the vortex formation due to the convective velocity of the vortex that is estimated to be 0.35-0.4 U_∞ in agreement with Carr et al. [14].

In order to further analyse the behavior of the wake for the light and deep dynamic stall conditions, Figures 6-7) show the evolution of the adimensional freestream velocity defect

$\hat{U}_{def}$ and of the turbulence intensity $\hat{u}'$ during the pitching cycle, where

$$\hat{U}_{def} = 1 - \frac{\langle U \rangle}{U_\infty}; \qquad \hat{u}' = \frac{\sqrt{\langle u'u' \rangle}}{U_\infty}. \tag{5}$$

During light dynamic stall condition the defect velocity region moves along the test section height direction showing the wake oscillations. The maximum values of the $\hat{U}_{def}$ are in the order of $7 - 10\%$ U_∞. The more extended region of the velocity defect observed during the downstroke demonstrates a thickening of the wake in this phase of the motion (see Fig. 6(a)). The peak of the turbulence intensity in downstroke ($= 0.06$) is twice than the one evaluated in upstroke (see Fig. 7(a)).

For the deep dynamic stall condition, the behavior of the velocity defect during the upstroke is similar to the one observed for the light dynamic stall condition tested. During the downstroke motion, the behavior of the adimensional velocity defect illustrates the conspicuous thickening of the wake produced by the large vortical structures detached from the airfoil trailing edge peculiar of this flow regime (see Fig. 6(b)). The peak of the turbulence intensity for this test case reaches the value of 0.25 (see Fig. 7(b)).

Figures 8 and 9 present the difference of the phase averaged pressure measured upstream and downstream the airfoil both on the ceiling and the floor of the test section for the tested conditions.

As can be observed, the measured values of the pressure differences on the ceiling and the floor of the test section are different due to the pitching airfoil motion; in particular, the pressure difference grows increasing the angle of attack for both the tested conditions.

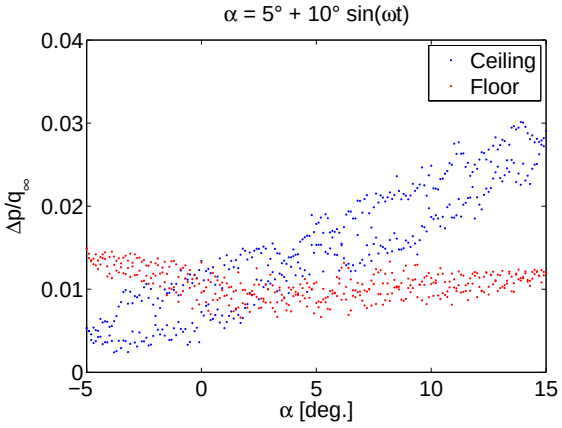

Figure 8: Pressure difference measured upstream and downstream the airfoil for the Light Dynamic Stall condition.

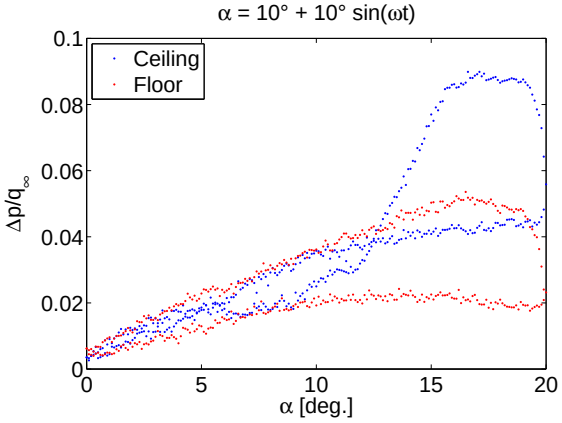

Figure 9: Pressure difference measured upstream and downstream the airfoil for the Deep Dynamic Stall condition.

5 Evaluation of drag coefficient

The measured wakes can be used to estimate the airfoil drag evolution during the pitching period. Due to both the strong unsteadiness and the not negligible degree of three-dimensionality a correct application of the integral equation of Navier-Stokes would require more information than it is actually available from the present measurements. On the other hand, on the base of reasonable assumptions, an approximated estimation of the drag can be attempted.

In fact, the loads acting on an object invested by a flow can be evaluated from the integration of the flow physical properties inside a control volume V enclosing the object with external surface S [15].

The x-component of the integral incompressible Navier Stokes equation applied to the volume of Fig.10 is the following:

$$\rho \frac{d}{dt} \int_V u \, dV + \rho \int_S u(\mathbf{V} \cdot \mathbf{n}) dS = -D + \int_S \tau_{nx} dS \tag{6}$$

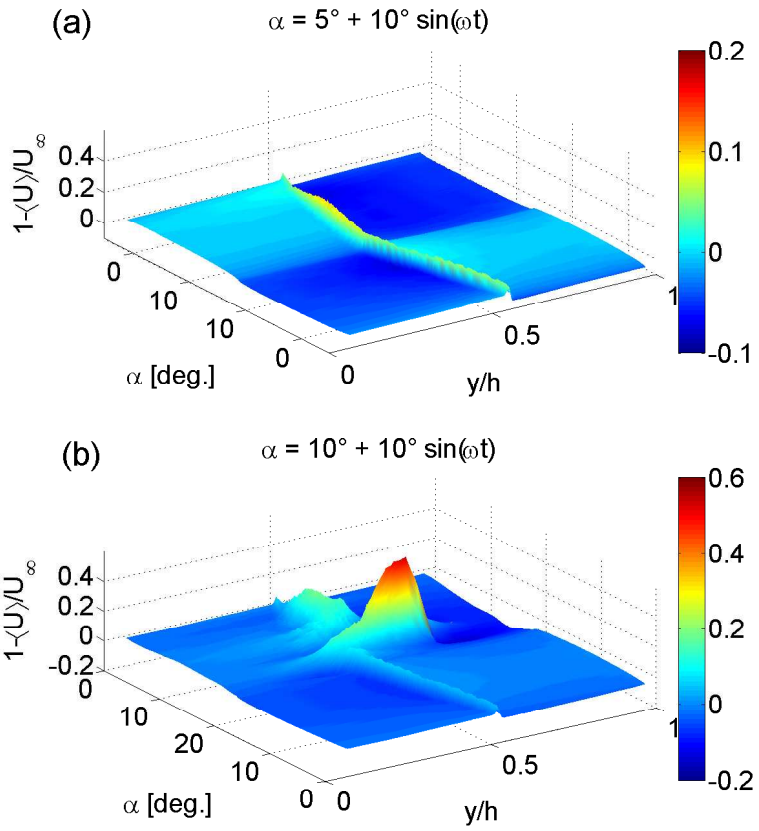

Figure 6: Freestream adimensional velocity defect for Light Dynamic Stall (a) and deep Dynamic Stall (b) condition.

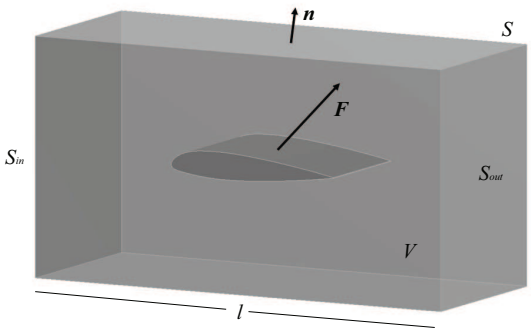

Figure 10: Control-volume for drag evaluation.

while the continuity equation is:

$$\int_S (\mathbf{V}\cdot\mathbf{n})dS = 0 \tag{7}$$

where S is the external surface and τ is the total stress (comprehensive of pressure and viscous stress). If the phase average operator is applied to this equation we obtain the following equations:

$$\begin{aligned}\rho\frac{d}{dt}\int_V \langle u\rangle dV + \rho\int_S \langle u\rangle(\langle\mathbf{V}\rangle\cdot\mathbf{n})dS + \\ \rho\int_S \langle u'(\mathbf{V}'\cdot\mathbf{n})\rangle dS = -\langle D\rangle + \int_S \langle\tau_{nx}\rangle dS,\end{aligned} \tag{8}$$

$$\int_S (\langle\mathbf{V}\rangle\cdot\mathbf{n})dl = 0. \tag{9}$$

Let us assume (as done by van Dam [9]) that there is not flow through the upper and lower sides of the control volume and that the inlet side S_{in} is far enough upstream to assume uniform conditions. In particular in the present work the inlet and outlet surfaces of the control volume are positioned in correspondence of the pressure ports position on the floor and the ceiling of the test section, respectively 3 chords ahead the airfoil leading edge and 2 chords past the airfoil trailing edge, and are considered with

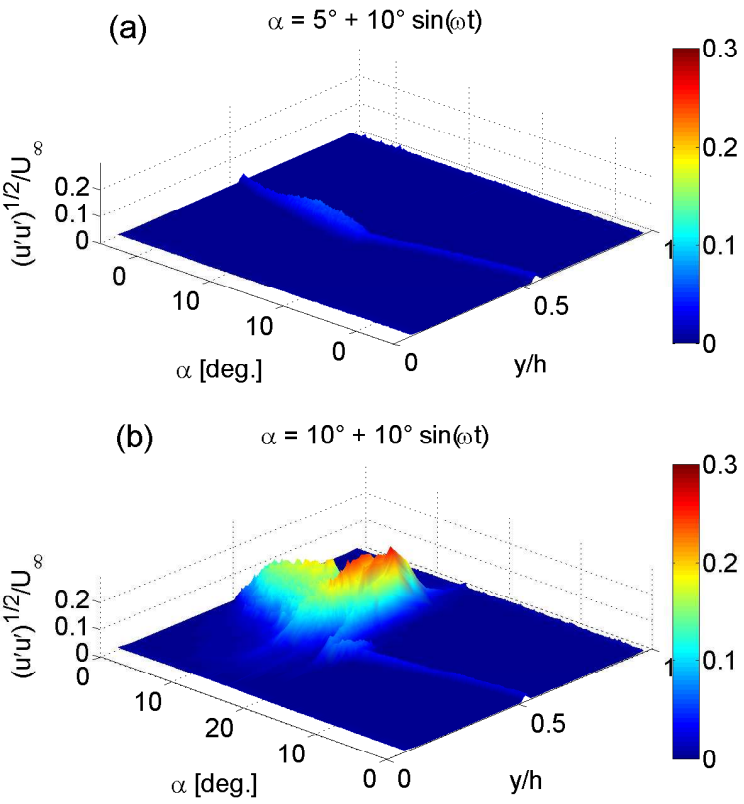

Figure 7: Freestream turbulence intensity for Light Dynamic Stall (a) and Deep Dynamic Stall (b) condition

equal area. This corresponds, due to the lack of boundary layer measurements in these tests, to assume that the slight test section divergence completely balances the increase of the boundary layer displacement thickness. With these hypotheses, making the different contributions explicit, the momentum equation becomes:

$$-\langle D\rangle + \int_{S_{out}} (p_\infty - \langle p\rangle + 2\mu\frac{\partial\langle u\rangle}{\partial x})dS = lS_{in}\rho\frac{dU_\infty}{dt} + \rho\int_{S_{out}}(\langle u\rangle^2 - U_\infty^2)dS + \rho\int_{S_{out}}\langle u'u'\rangle dS. \quad (10)$$

as

$$\int_l\int_S(\langle u\rangle dSdl = lU_\infty S_{in}. \quad (11)$$

In the present work the time derivative of the free-stream velocity was considered negligible together with the normal viscous stress component and the velocity fluctuation term. Moreover, the velocity profile measured in the wake of the airfoil at the model midspan plane was assumed uniform along the outlet surface of the control volume (2D flow assumption).

Equation (10) requires the measurement of the pressure distribution in the wake. The accurate measurement of the pressure in an unsteady flow field, as for the case of the wake of a pitching airfoil, is a critical point. Consequently, for the present activity the pressure term on the outlet side was obtained from the integration of Navier Stokes momentum equation using the measured velocity distribution. The differential form of Navier-Stokes momentum equation in y-direction can be written, for the present case, as follows:

$$\rho\frac{\partial\langle v\rangle}{\partial t}+\rho\langle u\rangle\frac{\partial\langle v\rangle}{\partial x}+\rho\langle v\rangle\frac{\partial\langle v\rangle}{\partial y}=-\frac{\partial\langle p\rangle}{\partial y}+$$
$$\mu(\frac{\partial^2\langle v\rangle}{\partial x^2}+\frac{\partial^2\langle v\rangle}{\partial y^2})-\rho\langle u'\frac{\partial v'}{\partial x}\rangle-\rho\langle v'\frac{\partial v'}{\partial y}\rangle. \quad (12)$$

As a further approximation the Taylor hypothesis was assumed leading to consider equal to zero the sum of the first two terms on the left side in Eq. 12. Moreover, also the second derivative of the velocity in freestream direction as well as the velocity components fluctuation terms were considered negligible. The pressure gradient in y direction from the simplified Eq. 12 was integrated using as starting points both the pressure measured on the floor and the pressure measured on the ceiling of the test section; the calculated pressure profiles were averaged to obtain the pressure profile at the outlet side of the control volume in Eq. 10. As for the velocity profile, also the calculated pressure profile was assumed two-dimensional.

Pressure on the inlet surface was considered uniform and equal to the mean of the phase averaged pressures measured on the floor and the ceiling of the test section.

Figures 11 and 12 show the total drag coefficients calculated for the light and the deep dynamic stall tested conditions compared to the pressure drag coefficient evaluated by pressure measurements on the airfoil contour.

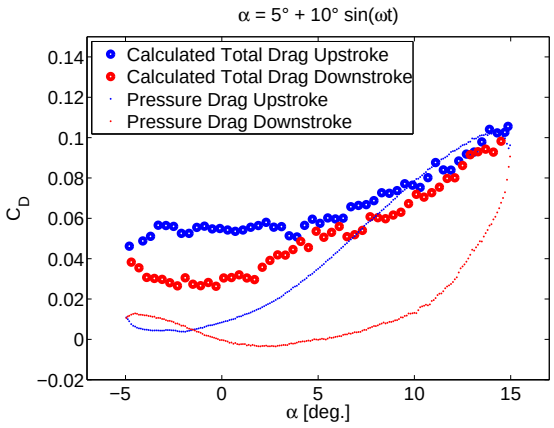

Figure 11: Comparison between the total drag coefficient and the pressure drag coefficient for the Light Dynamic Stall condition.

The calculated total drag presents higher values than the measured pressure drag contribution, in particular at low angles of attack. Increasing the angle of attack, the calculated drag approaches the value of the pressure drag component as expected; in fact, at high angles of attack, the drag contribution due to the viscous stresses can be considered negligible. For the deep dynamic stall condition the drag coefficients calculated in the range $12° < \alpha < 18°$ in downstroke are not presented in Fig. 12 due to the fact that in this phase of the pitching cycle strong three-dimensional secondary flows occur, as can be seen from Fig. 14 where the bulk velocity integrated along the velocity profile is presented: the bulk velocity defect observed from $12° < \alpha < 18°$ in downstroke demonstrates that the flow is quite three-dimensional for this angle of attack range.

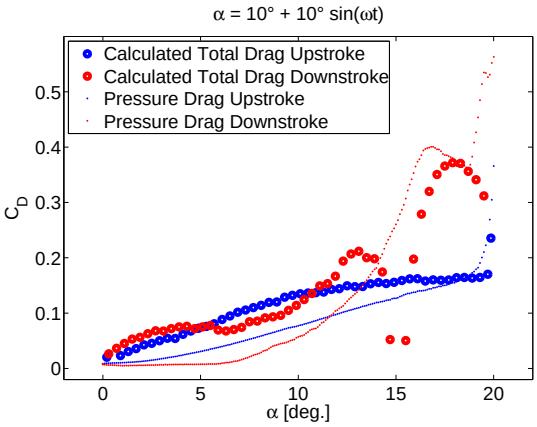

Figure 12: Comparison between the total drag coefficient and the pressure drag coefficient for the Deep Dynamic Stall condition.

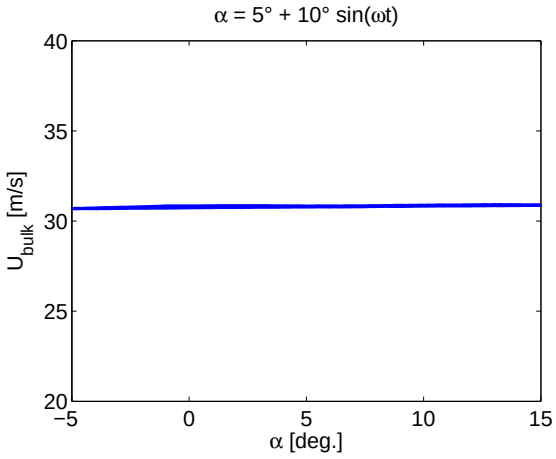

Figure 13: Wake bulk velocity for the Light Dynamic Stall condition.

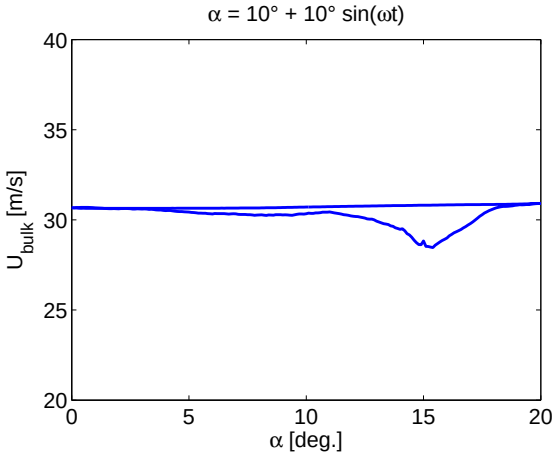

Figure 14: Wake bulk velocity for the Deep Dynamic Stall condition.

6 Conclusions

An extensive wake survey was carried out downstream of a pitching airfoil in light and deep dynamic stall. The results will be used for comparison with numerical simulations to evaluate the phase averaged total drag. A preliminary drag evaluation was carried out by use of the integral form of Navier Stokes equation under approximated assumptions.

References

[1] W.J. McCroskey. The Phenomenon of Dynamic Stall, NASA TM 81264, 1981.

[2] J.G. Leishman. Principles of helicopter aerodynamics, Cambridge Aerospace Series, 2000.

[3] K. Mulleners and M. Raffel. The Onset of Dynamic Stall Revisited, *Experiments in Fluids*, **52**, 779-793, 2012.

[4] M. Raffel, J. Kompenhans, B. Stasicki, B. Bretthauer and G.E.A. Meier. Velocity measurement of compressible air flows utilizing a high-speed video camera, *Experiments in Fluids*, **18**, 204-206, 1995.

[5] J. W. Chang. Near-Wake Characteristics of an Oscillating NACA 4412 Airfoil, *Journal of Aircraft*, **41**, 1240-1243, 2004.

[6] H. Sadeghi, M. Mani, M. A. Ardakani. Effect of Amplitude and Mean Angle of Attack on Wake of an Oscillating Airfoil, *Proceedings of World Academy of Science, Engineering and technology*, **33**, 125-129, 2008.

[7] A. Betz. A Method for the Direct Determination of Wing Section Drag, NACA TM 337, 1925.

[8] B.M. Jones. Measurement on Profile Drag by the Pitot-Traverse Method, British ARC R&M 1688, 1936.

[9] C.P. van Dam. Recent Experience with Different Methods of Drag Prediction, *Progress in Aerospace Sciences*, textbf35, 751-798, 1999.

[10] A. Zanotti, F. Auteri, G. Campanardi and G. Gibertini. An Experimental Set Up for the Study of the Retreating Blade Dynamic Stall, 37th European Rotorcraft Forum, 13-15 September, Gallarate (VA), Italy, 2011.

[11] J.G. Leishman. Dynamic stall experiments on the NACA 23012 aerofoil, *Experiments in Fluids*, **9**, 49-58, 1990.

[12] A. Zanotti and G.Gibertini. Experimental investigation of the dynamic stall phenomenon on a NACA 23012 oscillating airfoil, Proceedings of the Institution of Mechanical Engineers, Part G: Journal of Aerospace Engineering, first published on July 20, 2012, doi:10.1177/0954410012454100.

[13] P. Wernert and D. Favier, Considerations about the phase averaging method with application to ELDV and PIV measurements over pitching airfoils. *Experiments in Fluids*, **27**, 473-483, 1999.

[14] L.W. Carr, K.W. McAlister and W.J. McCroskey. Anaysis of the Developmentn of Dynamic Stall Based on Oscillating Airfoil Experiments, NASA TN D-8382, 1977.

[15] J.D. Anderson jr. Fundamentals of aerodynamics, 2nd edn. McGraw Hill, New York, 1991.